Environmental Science Nano

Stability of $Ti_3C_2T_x$ MXenes in Engineered Environments

Journal:	*Environmental Science: Nano*
Manuscript ID	EN-ART-06-2023-000438.R2
Article Type:	Paper

The fate and range of applications for MXenes in aqueous conditions requires an assessment of their behavior in various engineered environments, such as those generated by UV radiation and oxidants used in drinking water and membrane treatment strategies. Our findings indicate that while titanium carbide MXenes are stable at circumneutral pH and in the presence of UV radiation they are susceptible to transformations when exposed to oxidizing conditions created by free chlorine, leading to their effective conversion to crystalline TiO_2. Based on typical chlorine levels used in drinking water this corresponds to an approximate half-life of 19 to 5 h for MXenes at pH 7. In the context of using MXenes for membrane applications, our results highlight the need to develop surface modification processes capable of maintaining their stability under harsh oxidizing conditions while retaining their desirable physicochemical properties.

Stability of $Ti_3C_2T_x$ MXenes in Engineered Environments

Nasim Ganji[1], Christian A. Reardon-Lochbaum[1], Swapnil B. Ambade[2], Caroline M. Anastasia[3], Patrick M. Eckhert[3], Zeev Rosenzweig[2], Joel A. Pedersen[1,4,5], D. Howard Fairbrother[3,*]

[1]Department of Chemistry, University of Wisconsin−Madison, Madison, Wisconsin 53706, United States

[2]Department of Chemistry and Biochemistry, University of Maryland Baltimore County, Baltimore, MD 21250, United States

[3]Department of Chemistry, Johns Hopkins University, Baltimore, MD 21218, United States

[4]Departments of Soil Science and Civil & Environmental Engineering, University of Wisconsin−Madison, Wisconsin 53706, United States

[5]Department of Environmental Health and Engineering, Johns Hopkins University, Baltimore, Maryland 21218, United States

KEYWORDS: 2D material, $Ti_3C_2T_x$ MXene, UV, chlorine, stability, oxidation

ABSTRACT

MXenes are a newer class of 2D materials with desirable properties making them attractive for various environmental applications, including remediation and as membranes for water treatment. Until recently, the practical implementation of MXenes was hindered by their instability in water, although improved synthesis procedures have addressed this issue. Consequently, it is now important to assess the stability of MXenes in engineered environments relevant to drinking water and membrane operation (e.g. backwashing). In this study, $Ti_3C_2T_x$ MXenes were found to remain stable upon exposure to an aqueous environment saturated with oxygen and to UVC and UVA light at circumneutral pH, but were transformed upon exposure to excess free chlorine and to Fe(III) chloride at a concentration equal to 5 $mg \cdot L^{-1}$ free chlorine. The chlorination reaction kinetics are 1st order with respect to $Ti_3C_2T_x$ and free chlorine concentration from 20-200 $mg \cdot L^{-1}$. The rate constant increased at pH $\leq$ 7.5, implicating HOCl as the reactive species. We propose that MXene reactions with HOCl occur by an electrophilic attack of Cl^+, forming TiO_2 and degrading the MXene. AFM data shows that transformations are initiated at the edges of the MXene sheets and localized areas on the MXene, suggesting that the initial sites for Cl^+ attack are defect sites and/or uncoordinated Ti atoms. This contrasts with the inertness of nanoscale TiC, highlighting the need to devise surface modification processes that will allow MXenes to resist the oxidative conditions associated with membrane regeneration/backwashing.

INTRODUCTION

Two-dimensional transition metal carbides, nitrides, and carbonitrides (MXenes) are defined by the general chemical formula $M_{n+1}X_nT_x$, where M is an early transition metal, X is C and/or N, T represents various possible basal plane terminations (most commonly –OH, –O, and/or

–F), and *x* indicates the number of surface functionalities.[1,2] Metallic conductivity, coupled with desirable mechanical properties, hydrophilicity, and high surface area to volume ratios make MXenes of interest for a variety of contaminant remediation and water treatment applications.[3–13]

Within the MXene family, titanium-based MXenes such as Ti_2CT_x and $Ti_3C_2T_x$ are the most promising for these types of environmental applications due to availability and biocompatibility.[4,14–20] In particular, $Ti_3C_2T_x$ along with its composites have demonstrated excellent properties in adsorption and rejection of ions, dyes, heavy metals, and radionuclides.[21–23] More recently, 2D $Ti_3C_2T_x$ MXenes with atomic thickness have been extensively investigated as building blocks of high-performance membranes engineered on a nanometer or even sub-nanometer scale.[24] Thus, $Ti_3C_2T_x$ MXene membranes with nanometer-scale channels have enabled efficient and controlled rejection/permeation of inorganic ions and organic dye molecules based on permeation selectivity toward cations of various sizes and charges, while the hydrophilic nature of $Ti_3C_2T_x$ accompanied by H_2O between layers promotes ultrafast water flux.[24,25] Graphene and graphene oxide (GO) derivatives, which are similar 2D materials, have also demonstrated exceptional performance as water purification membranes with unique properties, such as ultra-high water flux, selective molecular and ion sieving, and strong resistance to biofouling.[26] However, MXenes have several significant advantages over graphene and other conducting nanomaterials. MXenes form stable colloidal solutions without additives or surfactants, and they can easily be processed using the cheapest and safest solvent: water.[27] Moreover, $Ti_3C_2T_x$ membranes have demonstrated better performance than GO in the separation of higher charge cations.[28,29] Further, MXenes could be used as active components in conductive membranes and would likely exhibit many of the same benefits previously shown for membranes containing

conductive carbon nanotubes (e.g. improved biofouling resistance and redox-activated remediation capabilities). [22,23]

Given the relative newness of MXenes, many uncertainties exist about their long-term stability in natural or engineered environments. Earlier studies have shown that MXenes can be prone to oxidation and last no longer than a few weeks when stored as aqueous suspensions.[30–35] However, synthetic strategies have been recently developed to significantly reduce their oxidation rates and form stable colloids in water.[27,33,36–38] The motivation behind our work stems from the need to address these uncertainties and advance the understanding of MXenes' stability in specific engineered environments, such as those present in water treatment facilities or those they will encounter if used in membranes. These include, but are not limited to, the engineered environments investigated in this paper; chlorination, UV-radiation, Fe(III) chloride, and saturated/dissolved oxygen. Chlorine and UV-radiation are used to disinfect drinking and waste water, oxygen is added to stimulate microorganisms to degrade organic matter, an important component in aerobic wastewater treatment[39,40] and Fe(III) chloride is used as a mild oxidant and flocculant.[41] This information is needed to assess the fate of MXenes in aquatic environments and also to identify the extent of their potential applications.

In engineered environments, one of the most commonly used oxidants is chlorine, which is used to disinfect water and is part of the sanitation process for sewage and industrial waste.[42] Chlorine is also commonly applied to remove impurities (foulants) that form on membrane surfaces due to its low cost, wide availability, and high efficacy in fouling mitigation.[43,44] In some scenarios, a high concentration of chlorine is applied (e.g., up to 5×10^4 ppm·h), for which the chemical stability of the membrane is crucial in determining its effective lifetime.[45–47] Chlorine, either in its molecular form (Cl_2) or as hypochlorite salts (NaClO), forms hypochlorous acid

(HOCl) and hypochlorite ions (OCl^-) during disinfection, which are the main oxidative compounds and are known to react and transform numerous inorganic and organic compounds.[48,49] In the presence of sunlight or UV irradiation, free chlorine can also generate radical species such as $^{\bullet}Cl$ and $^{\bullet}OH$, which can subsequently lead to the formation of other oxygen and/or chlorine-based radicals.[50]

This study focuses on understanding the reactivity and stability of $Ti_3C_2T_x$ MXenes with UV irradiation (254 and 365 nm) and free chlorine as a function of pH, free chlorine concentration, and the presence of UV irradiation. As free chlorine is a common engineered environment when it comes to water treatment, we conducted extensive characterization of MXene transformation due to chlorination. We also evaluated the stability of $Ti_3C_2T_x$ in saturated oxygen solutions and Fe(III) chloride with UV-vis spectroscopy. Detailed product characterization was performed using atomic force microscopy (AFM), X-ray photoelectron spectroscopy (XPS), X-ray diffraction (XRD), energy dispersive X-ray spectroscopy (EDS), and scanning electron microscopy (SEM). Our results show that while MXenes are inert to UV radiation and saturated oxygen, they are susceptible to degradation in the presence of stronger oxidants such as Fe(III) chloride and free chlorine. In the presence of free chlorine, reactions proceed at defects and edge sites of $Ti_3C_2T_x$ MXenes to produce amorphous TiO_2 sheet-like structures that are further transformed to nanocrystalline TiO_2 particles.

EXPERIMENTAL

Materials. Ti_3AlC_2 MAX phase was procured from the Gogotsi Group, Drexel University, USA. Hydrofluoric acid (48 wt % in H_2O, ≥ 99.9% trace metals basis), hydrochloric acid (37%), lithium chloride (≥ 99.9%), sodium phosphate monobasic (≥ 99.0%), sodium hydroxide (50% in

H_2O), nitric acid (65−71%, TraceSELECT Ultra grad), titanium (IV) carbide (nanopowder, < 200 nm, ≥ 99%), Iron (III) chloride (97%), and standard titanium solution (1000 $mg \cdot L^{-1}$ in nitric acid, TraceCERT) were purchased from Sigma Aldrich. Sodium hypochlorite (5% chlorine) was purchased from Acros Organics. Oxygen gas was purchased from AirGas (UHP200). All chemicals were reagent grade unless otherwise noted and used as received except for sodium hypochlorite, which was standardized using a HORIBA Aqualog optical spectrometer (ε_{292} = 359 $M^{-1} \cdot cm^{-1}$). Ultrapure water (resistivity 18.2 MΩ·cm) was produced by a GenPure Pro UV-TOC/UF system (Thermo Fisher Scientific, Waltham, MA, USA).

$Ti_3C_2T_x$ synthesis. We synthesized $Ti_3C_2T_x$ MXene nanosheets following the procedure described previously.[51] In brief, 1 g of the Ti_3AlC_2 was mixed with 10 mL of etchant and stirred at 500 rpm for 24 h at 35 °C. The etchant was a 6:3:1 mixture (by volume) of 12 M HCl, DI water, and 48 wt % HF. The etched $Ti_3C_2T_x$ was then washed with MilliQ water by repeated centrifugation at 3500 rpm and decantation cycles until the supernatant reached neutral pH. Once the MXene solution was neutralized, an additional wash cycle was performed to ensure the washing process was complete. The produced multilayered MXene sediment was redispersed in a 1.2 M solution of LiCl and delaminated by stirring at 300 rpm for 24 h, at room temperature. The MXene/LiCl suspension was then washed by repeated centrifugation and decantation of supernatant. The washing procedure was repeated until the colloidal MXene solution was stable. The solid content of the supernatant was determined by vacuum drying a known solution volume and measuring the weight of the resulting MXene powder upon drying in a freeze-dryer overnight.

Photochemical stability. The photochemical stability of colloidal $Ti_3C_2T_x$ was assessed in quartz test tubes (VWR 89063-442, 1 cm in diameter) either covered with aluminum foil to prevent irradiation or placed into a Rayonet photochemical reactor (RPR100, Southern New England

Ultraviolet Co. Branford, CT). The Rayonet photochemical reactor was equipped with a fan and either four 254 nm bulbs (RPR-2537A, fluence = 7.30×10^{-3} mE·cm^{-2}) or sixteen 365 nm bulbs (RPR-3500A, fluence = 6.36×10^{-2} mE·cm^{-2}).[52] These bulbs were selected because they represent distinct regions in the ultraviolet spectrum, i.e., 365 nm (UVA); 254 nm (UVC) and are not monochromatic sources, identified by the λ_{max}.

Chlorination experiments. Free chlorine was created by adding NaOCl to $Ti_3C_2T_x$ solutions. The pH of the system was adjusted initially to 5, 6, 7, 8, 9, or 10 by nitric acid (HNO_3) and/or sodium hydroxide (NaOH) and unless noted stabilized with 10 mM phosphate buffer (NaH_2PO_4). For single concentration chlorine exposure experiments, chlorine was added to MXene solutions at 50 mg·L^{-1}. For kinetics experiments, chlorine was added from 20-200 mg·L^{-1}. Chlorine concentrations in drinking water applications range from 1-4 mg·L^{-1}, so the concentrations used in this study exceeded those found in drinking water disinfection to accelerate the effects of chlorine on MXenes. Concentrations were calculated assuming 5% free chlorine in the stock. As the reaction proceeded, 2 mL sample aliquots were taken at specific time intervals and immediately analyzed using a HORIBA Aqualog optical spectrometer to monitor $Ti_3C_2T_x$ absorbance changes. As established by Zhang et al.,[33] the UV–vis absorbance peak around 780 nm is a relative measure of $Ti_3C_2T_x$ concentration in solution and was used to evaluate reaction kinetics.[27,33] All experiments were conducted in triplicate at room temperature (21.0 ± 1.0 °C). Control exposures of $Ti_3C_2T_x$ with no free chlorine at the same pH were also conducted. Sample aliquots were collected at specific reaction times and analyzed by inductively coupled plasma mass spectrometer (ICP-MS), atomic force microscopy (AFM), X-ray photoelectron spectroscopy (XPS), X-ray powder diffraction (XRD), and scanning electron microscopy and energy dispersive

X-ray spectroscopy (SEM-EDS). Further details on the characterization of $Ti_3C_2T_x$ MXene and reaction products are provided in the Supporting Information (SI).

Stability in oxygen saturated and Fe(III) chloride solutions. Fe(III) chloride experiments were carried out by adding 7.05×10^{-5} M Fe(III) chloride, or the molar equivalent to 5 $mg \cdot L^{-1}$ Cl_2, to a 25 $mg \cdot L^{-1}$ solution of $Ti_3C_2T_x$ MXenes and measuring the UV-Vis absorbance as a function of time. $Ti_3C_2T_x$ oxygen saturation experiments were conducted by continuously bubbling oxygen into a 25 $mg \cdot L^{-1}$ solution of $Ti_3C_2T_x$ MXenes and measuring the UV-Vis absorbance as a function of time; these data are provided in the Supporting Information (SI).

Product characterization in chlorination experiments. Prior to analysis, pristine and reacted $Ti_3C_2T_x$ samples were washed by centrifugation and rinsing with MilliQ water to remove any complicating salts, reactants, buffer, and possible small products. The pellets were then resuspended in DI water and drop cast on SiO_2 wafers (University Wafer) for analysis by AFM, XPS, and SEM. AFM images were collected in Soft Tapping mode using a Dimension Icon Atomic Force Microscope (Bruker) equipped with silicon tips (Bruker, RFESP-75). Image processing and height analysis were conducted with Gwyddian 2.61. XPS spectra were collected using a Thermo Fisher Scientific K-Alpha X-ray Photoelectron Spectrometer with an Al Kα source (1486.6 eV photon energy) at a 45° take-off angle. Survey spectra were taken at pass energy of 100 eV and resolution of 1.00 eV/step. For the C 1s, Ti 2p, O 1s, F 1s, and Cl 2p peaks, we used 50 eV pass energy and 0.20 eV/step resolution. To evaluate the atomic concentration of different elements throughout the films, samples were depth profiled with Ar^+ ion beam. The Ar^+ ion energy was 2 kV, and the beam emission current was 10 mA. The etching time step was 30 s. After each etch cycle, the ion beam was blanked, and an XPS spectra was recorded.

XRD patterns were obtained using a Bruker D8 ADVANCE powder X-ray diffractometer with a Cu Kα source and a Lynxeye detector. Concentrated dispersions of pristine and reacted $Ti_3C_2T_x$ in isopropyl alcohol were prepared through ultrasonication. The mixture was then drop-cast onto a zero-diffraction plate (MTI Corp) and allowed to dry, forming a uniform film. Diffraction patterns were recorded from 3−65° with a step size of 0.02° and dwell time of 1 s at each point. XRD patterns for TiO_2 (anatase) powders were obtained under the same analysis conditions for comparison.

EDS analysis was performed with a JEOL EDS detector in a JSM-IT100 scanning electron microscope at 10 kV accelerating voltage. An acceleration voltage of 10 kV was selected to enable the use of Ti-K x-rays for quantification to avoid using the Ti-L signals, which overlap with C-Kα and O-Kα. In order to generate films of sufficient thickness for EDS analysis, several drops from concentrated dispersions of pristine and reacted $Ti_3C_2T_x$ were placed on Si wafers and dried under a stream of nitrogen gas. Due to significant peak overlap in the region for the X-ray lines of carbon, oxygen, and titanium, simulated spectra were compared to experimental data to determine the approximate composition of the MXene. The open-source software DTSA-II from the National Institute of Science and Technology was used to simulate spectra. Using a collected spectrum of TiO_2, the software was calibrated to approximate the JEOL EDS detector. Spectra were then simulated for materials containing primarily Ti, C, and O with trace F and Cl. The compositions were iteratively modified until the simulated spectra qualitatively reflected the appearance of the experimentally collected spectra. Due to low fluorescent yields of low energy X-rays and significant secondary fluorescence and self-absorption, the results of C and O analysis should be viewed conservatively, particularly in a material with characteristic x-rays that overlap C and/or O, e.g., Ti-L x-rays near 450eV.

The supernatant was analyzed by UV-vis to measure the final concentration of free chlorine in the solution and identify the extent of chlorine consumption. The solution pH was first set to 11; the absorbance at 292 nm[53] was then measured and referenced to the molar absorptivity (absorption coefficient) of OCl^- at 292 nm (ε_{292} = 359 $M^{-1}\cdot cm^{-1}$ at pH 11).[53] The supernatant was further examined by ICP-MS (Agilent 8900) to evaluate the release of titanium ions from $Ti_3C_2T_x$ during the chlorination process. Before the measurements, supernatant samples were acidified to 2% nitric acid to solubilize the metal and then were diluted 10 times with DI water. Standard solutions containing 1, 10, 100, 500, and 1000 $\mu g\cdot L^{-1}$ Ti dissolved in 2% nitric acid were used for instrument calibration. All measurements were conducted in triplicate.

RESULT AND DISCUSSION

Characterization of $Ti_3C_2T_x$ nanosheets. XRD, XPS, and AFM were used to confirm the complete removal of Al layers from the MAX phase, and the structure and morphology of the MXene flakes. As shown in Figure 1A, after selective etching, the (014) peak at $2\theta \approx 39°$ in the XRD pattern of Ti_3AlC_2 disappeared which indicates the removal of Al layers from the MAX phase.[54] The absence of an Al 2p peak in XPS of as-prepared $Ti_3C_2T_x$ confirmed the complete removal of aluminum. Moreover, the broadening and shifting of the (002) $Ti_3C_2T_x$ nanosheet diffraction peak to a lower angle compared to bulk Ti_3AlC_2 was attributed to the expansion in interlayer spacing (Δd-spacing = 2.3 Å) caused by replacing Al atomic layers with functional groups (–O–, –OH, or –F) and the incorporation of water and ions.[55–57] The morphology of the flakes was evaluated by AFM. Figure 1B shows a representative AFM image of as-prepared $Ti_3C_2T_x$ flakes on a Si/SiO_2 substrate. The flakes are several micrometers in size, have smooth edges and uniform surfaces, and bear no visible signs of degradation. The AFM height profile

shows that the monolayer $Ti_3C_2T_x$ nanosheets has a thickness of ~ 2.1 nm, consistent with the reported thickness of a single layer $Ti_3C_2T_x$ (2.7 nm).[58]

$Ti_3C_2T_x$ colloids. To evaluate the stability of $Ti_3C_2T_x$ colloids suspended in phosphate buffer, UV-vis spectra were taken periodically over a 7-day period. Results for pH 6 are shown in Figure S1. No noticeable change in the UV-vis spectra of $Ti_3C_2T_x$ was observed after 7 days of storage in the dark and at room temperature, indicating the high stability of MXenes in the absence of free chlorine. This is attributed to the quality of the Ti_3AlC_2 MAX phase precursor used to produce $Ti_3C_2T_x$ nanosheets. Earlier studies revealed that $Ti_3C_2T_x$ MXenes produced from Ti_3AlC_2 are susceptible to oxidation and degrade in a week when stored as aqueous suspensions,[32,33] with the instability attributed to defects created during synthesis.[27,31] Mathis et al. have shown that including excess aluminum during the synthesis of Ti_3AlC_2 reduces the number of defects in the MAX phase. This leads to Ti_3AlC_2 grains with improved Ti:C stoichiometry, which in turn results in less defective $Ti_3C_2T_x$ which is highly stable in aqueous solutions and in air.[27] Colloidal $Ti_3C_2T_x$ MXene is, however, observed to react with free chlorine. As shown in Figure 2A, characteristic $Ti_3C_2T_x$ peaks at 320, and 780 nm[59] disappeared over the course of 70 minutes of exposure to free chlorine, with the initially black colored solution becoming transparent (Figure 2B).

MXene degradation. To quantify chlorine induced degradation, UV-vis spectra of $Ti_3C_2T_x$ were taken at 10 minute intervals over 70 minutes (Figure 2A).[27,33] As shown in Figure 2C, for $Ti_3C_2T_x$ exposed to 50 $mg \cdot L^{-1}$ free chlorine, the normalized absorbance at 780 nm decreased steadily over time, indicating the degradation of $Ti_3C_2T_x$.[60] Figure 3A shows how the MXene concentration changed as a function of time in the presence of different chlorine concentrations (20 to 200 $mg \cdot L^{-1}$) at pH 6, revealing that the MXene degradation rate increases systematically as the chlorine concentration increases. The data in Figure 3A was analyzed to

determine the reaction kinetics. Since both the MXene and chlorine concentrations were changing, the analysis was restricted to the initial period of MXene loss (t < 10 min), where the chlorine concentration would remain relatively unchanged from its initial value. Under these conditions the rate of loss of MXene was hypothesized to follow a 1st order kinetic dependence:

$$\frac{d[\text{MXene}]}{dt} = -k'[\text{MXene}] \quad (1)$$

The apparent rate constant (k′) for each free chlorine concentration was determined by linear regression of $\ln([\text{MXene}]_t/[\text{MXene}]_0)$ versus time. Figure 3B shows that the initial rate of MXene loss can be well fit by first order reaction kinetics, while Figure 3C reveals that the k′ value is proportional to the initial free chlorine concentration. Thus, the overall relative reaction kinetics are 1st order with respect to $Ti_3C_2T_x$ and free chlorine, and can be described by the following equation:

$$\frac{d[\text{MXene}]}{dt} = -k\,[\text{MXene}][\text{Chlorine}] \quad (2)$$

These findings are similar to those of An et al. who found that the reaction kinetics of graphene oxide (GO) with free chlorine under both dark and ultraviolet (UV) irradiation are second order overall; first order with respect to both GO and initial chlorine concentrations.[61] It should be noted that at relatively low initial free chlorine concentrations (e.g. 10 $mg \cdot L^{-1}$), the MXene concentration decreased until all of the free chlorine was consumed (Figure S2); thereafter, the UV-Vis was unchanged due to the stability of the remaining unreacted MXenes in the absence of free chlorine. Figure S2 also reveals that for an initial MXene concentration of 25 $mg \cdot L^{-1}$approximately 25 $mg \cdot L^{-1}$ free chlorine is required for complete MXene degradation as judged by the loss of absorbance at 780nm.

Impact of pH. In the presence of Cl_2, MXene reaction rates are highly sensitive to solution pH, with significantly faster reactions occurring at lower pH (Figure 4A). This trend is attributed to the different chlorine species (HOCl/OCl^-) present in solution under different pH conditions as presented in Eqs. (4) and (5):[62,63]

$$NaOCl + H_2O \rightarrow HOCl + Na^+ + OH^- \quad (3)$$

$$HOCl \rightleftharpoons H^+ + OCl^- \ (pK_a = 7.53 \text{ at } 25\ ^\circ C) \quad (4)$$

Upon introduction into solution, sodium hypochlorite immediately hydrolyzes to form hypochlorous acid (HOCl) which can then dissociate into hypochlorite (OCl^-) and hydrogen (H^+) ions. The extent of HOCl dissociation depends on the solution pH (Figure 4B). At lower pH levels, HOCl is the dominant species, while ClO^- is dominant at higher pH.[43,64] As shown in Figure 4C, reaction rate constants of $Ti_3C_2T_x$ with free chlorine correlate well with the relative concentration of HOCl in solution. A similar trend has been reported for the reaction of graphene oxide with free chlorine at varying pH,[61] consistent with a transformation process driven by hypochlorous acid.[49,64]

Impact of UV irradiation. In the absence of chlorine, no noticeable change in the UV-vis spectra of $Ti_3C_2T_x$ was observed under UV irradiation at either 254 nm (7.30×10^{-3} mE·cm^{-2}) or 365 nm (6.36×10^{-2} mE·cm^{-2}) indicating the photostability of MXenes (Figure 5A). In this respect, the photochemical stability of MXenes is in marked contrast to graphene oxide, which is known to undergo photochemical transformations.[65–67] Even if the UV light intensity in a commercial water treatment plant are orders of magnitude higher than the experiments described in this study, if we consider the volumes of water that must be disinfected each day in one of these plants it seems unlikely that UVC treatment alone will transform MXenes.

In the presence of both light and chlorine (50 mg·L^{-1}) $Ti_3C_2T_x$ did transform; at 365 nm MXene reaction rates were comparable to those in dark, while at 254 nm the rate of MXene

degradation decreased. This wavelength difference is attributed to the photoreactivity of HOCl at 254 nm as compared to 365 nm (Figure 5B), in line with its molar absorptivity (Figure S3).[52] The concentration of reactive chlorine species available to react with MXenes is depleted at 254nm, causing the reaction rate to decrease (Figure 5A). In contrast, there is no photodepletion of HOCl at 365 nm and the MXene reaction rate is unchanged upon irradiation (Figure 5A).

Product Characterization. Transformation products were colloidally stable and were isolated from the solution by centrifugation for analysis. In this way, $Ti_3C_2T_x$ MXenes were characterized by AFM after exposure to 50 $mg \cdot L^{-1}$ free chlorine at pH 6 for varying exposure times. Based on UV-Vis data, these exposure times corresponded to $[MXene]_t/[MXene]_0 = 1.00$, 0.75, 0.50, 0.25, and ≤ 0.05 defined as t_0, $t_{1/4}$, $t_{1/2}$, $t_{3/4}$, and t_f, respectively. AFM data shown in Figure 6A indicates that while pristine $Ti_3C_2T_x$ MXenes (t_0) had smooth edges and uniform surface roughness, the edges of MXenes after exposure to chlorine were significantly raised ($t_{1/2}$). Morphological transformations observed by AFM started predominantly on the edges and at localized regions on the basal plan, the latter assumed to be associated with defects. The extent of these structural transformations increased as the extent of MXene degradation increased (compare $t_{1/2}$ and $t_{3/4}$). AFM analysis also shows that although the single sheet MXene heights appeared to be unchanged (~2-3 nm) by their reactions with chlorine, the $t_{3/4}$ samples showed significantly more multi-sheet/aggregation behavior.

To further probe the transformation of $Ti_3C_2T_x$ flakes as a consequence of chlorination, XPS data were acquired at different stages of the reaction. High-resolution XPS spectra of the Ti 2p and C 1s regions at t_0, $t_{1/2}$, and t_f in are shown in Figures 6B and 6C, respectively. Spectral envelopes at t_0 are consistent with previous XPS data, with dominant peaks in the Ti 2p region at 456 and 461 eV (green bands in Figure 6B) corresponding to Ti $2p_{3/2}$ and $2p_{1/2}$ transitions of

$Ti_3C_2T_X$ MXene.[63,64] In the C 1s region (Figure 6C) the spectral envelope is dominated by a C–Ti peak at 281.8 eV (green band) and a peak at 284.8 eV associated with adventitious carbon, along with smaller peaks at higher binding energy (≈ 289 eV), likely due to more oxidized forms of carbon.[31] The survey spectra (0–1350 eV) contains contributions from O and F (Figure S4) due to the presence of Ti-OH and Ti-F surface functional groups.[36] Upon exposure to chlorine the peaks associated with the Ti–C decrease in intensity and new peaks at 458.6 eV and 464.5 associated with Ti (+4) appear.[33] In the survey spectra the O(1s) peak intensity also increases significantly, consistent with the formation of TiO_2. At $t_{1/2}$, where $[MXene]/[MXene]_0 = 0.50$, the TiO_2 peaks are comparable in intensity to the nascent titanium carbide peaks, while at t_f all spectral features in the C 1s and Ti 2p regions associated with Ti–C disappeared.

XPS depth profiles of $Ti_3C_2T_x$ MXenes flakes in the C 1s region following varying chlorine exposure times are shown in Figure S5. For the native MXene (t_0), the adventitious carbon peak at 284.8 eV is rapidly removed during sputtering leaving only the C–Ti peak at 281.8 eV, consistent with surface contamination. For MXenes exposed to chlorine, although there is initially no evidence of a C–Ti peak at 281.8 eV, this feature appears as a consequence of sputtering, leading to a C1s envelope that contains peaks at both 284.8 eV and 281.8 eV. Thus, although the surfaces of the MXenes were fully oxidized to TiO_2, some residual titanium carbide remains below the surface layers, while the persistence of the 284.8 eV peak throughout the sputtering process indicates that some form of graphitic or amorphous carbon is being formed as a consequence of chlorination. As the exposure time to chlorine increased, the concentration of Ti-C observed upon sputtering decreased; thus, after 7 days, the Ti–C peak had almost disappeared, along with an overall decrease in intensity in the C 1s region. Using the Ti-C peak as a measure of the MXene concentration in the MXene flakes, Figure S7 shows that upon sputtering the MXene concentration

increases until it reaches a steady state value, although the remaining MXene concentration decreases as chlorine exposure time increases.

The change in chemical composition after MXenes are exposed to chlorine was also studied by EDS. As shown in Figure 7A, chlorination led to a significant increase in oxygen, a decrease in carbon, and the loss of all fluorine. Due to significant peak overlap between the X-ray lines of carbon, oxygen, and titanium, simulated spectra were compared to experimental data to determine the approximate composition of the degraded MXene (compare Figure S8A and Figure S8B). In this way, after 1 day of chlorination, the O:Ti ratio was ~2.2 (Figure 7B), implying that most of Ti was in the form of TiO_2. Longer exposures to chlorine had no measurable impact on the composition of the film. Structural changes upon chlorination were also examined by monitoring the XRD patterns of $Ti_3C_2T_x$ as a function of chlorination time (Figure 7C). After one day of chlorination, an exposure sufficient to turn the solution colorless (see Figure 2), the disappearance of the (002) peak at $2\theta \approx 6°$ indicates the loss of MXenes, although the reaction products are non-crystalline. Longer exposure of $Ti_3C_2T_x$ to chlorine (i.e., 7 days), however, leads to an XRD pattern whose peak positions are indicative of crystalline anatase TiO_2.

The decrease in carbon within the reacted MXene flakes after chlorination is ascribed to CO_2 production.[68] This assertion is supported by the decrease in pH observed during the reaction of MXene with 50 $mg \cdot L^{-1}$ free chlorine in unbuffered DI (Figure S9). Moreover, the final pH was 3.72 ± 0.09, comparable to the pK_a of carbonic acid (3.49 ± 0.05) [68] and there is a good correlation between the rate of decrease in pH and the extent of MXene degradation measured by UV-Vis (compare Figure S9 and Figure 3A).

To determine if the transformation of $Ti_3C_2T_x$ result in the release of any Ti ions, pristine and reacted $Ti_3C_2T_x$ MXenes were sedimented by centrifugation, and the supernatant was analyzed

for [Ti] by ICP-MS. After exposure to free chlorine for one day, the concentration of Ti ions in solutions increased from 0.0131 ± 0.002 $mg \cdot L^{-1}$ to 0.9033 ± 0.176 $mg \cdot L^{-1}$. For context, the total Ti mass concentration in the $Ti_3C_2T_x$ colloidal suspensions (25 $mg \cdot L^{-1}$) calculated on the basis of EDS analysis was approximately 16.94 $mg \cdot L^{-1}$. Thus, approximately 5% of the nascent Ti in the MXenes is converted into Ti ions as a consequence of the transformations initiated by chlorination.

Reaction mechanism. Chlorine reactivity with anionic inorganic compounds is reported to occur by an initial electrophilic attack of HOCl. Hypochlorous acid reacts with an initial electrophilic attack via Cl^+ forming a reactive intermediate which is then rapidly hydrolyzed to an oxide.[49] We propose that the reaction of MXene occurs through an analogous mechanism, leading to the formation of TiO_2 and the degradation of the MXene, as evidenced by the UV-Vis data shown in Figure 2, supported by the XPS and EDS data in Figures 6B and 7A.

AFM data showing that transformations are initiated at the edges and localized areas on the MXene, suggests that the initial sites for Cl^+ attack are at higher energy sites, such as defects and/or uncoordinated Ti atoms that proliferate at the edges. In addition to TiO_2 and a small amount of aqueous Ti^{4+}, XPS data shows that some graphitic or amorphous carbon is formed, with some $Ti_3C_2T_x$ remaining below the topmost surface layer. After 1 day of chlorine exposure the TiC:C ratio is ≈ 35% based on the XPS C 1s peak fitting (Figure S7D), while EDS analysis indicates that the O:C ratio is ≈ 2.5. If we assume that the reaction products consist of a mixture of TiO_2, unreacted $Ti_3C_2T_x$ and graphitic/amorphous carbon, as described in the SI the XPS and EDS information allows us to propose that the initial reaction can be expressed as:

$$Ti_3C_2T_x + 4\ HOCl \rightarrow 2.82\ (Ti_3C_2T_x)_{0.07}(TiO_2)_{0.80}C_{0.13} + 0.15\ Ti^{+4} + 4\ Cl^- + 1.24\ CO_2 \quad (6)$$

Equation (6) captures the essence of the initial MXene degradation with the colloidally stable product retaining the sheet-like structure of the MXenes (as shown by SEM images in Figure

7E), being composed principally of TiO_2 along with some unreacted $Ti_3C_2T_x$ and amorphous or graphitic carbon. Considered collectively the XPS, AFM, and SEM data indicate that this initial transformation step results in some MXene aggregation, with the $Ti_3C_2T_x$ exposed at the surface or the edges of the aggregates undergoing oxidation leaving a small amount of $Ti_3C_2T_x$ in the interior of the aggregates remaining intact, as observed by XPS depth profiling (Figure S5).

After more prolonged exposures to chlorine (7 days at 50 $mg \cdot L^{-1}$ free chlorine) the EDS and XPS data show that only minor changes to the overall chemical composition of the reacted MXene flakes occur as the small amount of residual unreacted $Ti_3C_2T_x$ is slowly oxidized. However, as the chlorine exposure time increases from 1 day to 7 days the structure of the oxidized MXene flakes undergoes a solid-state transformation from a 2D sheet-like material as observed by AFM and SEM (Figures 6A and 7E) to crystalline anatase TiO_2 as evidenced by SEM (Figure 7F) and most clearly by XRD (Figure 7C). Evidence of this transformation is also apparent from the formation of a milky colored suspension, indicative of colloidal TiO_2 particles (Figure 7F inset). It should also be noted that in the absence of further chlorination beyond day 1, the reaction products remain non-crystalline after 7 days indicating that oxidation of the MXenes needs to be almost complete before crystallization can occur.

Having established that colloidal $Ti_3C_2T_x$ is unstable in the oxidizing conditions created by free chlorine (E_o = 1.36V), we also explored less oxidizing conditions present in engineered environments (Table S1). In this respect, $Ti_3C_2T_x$ MXenes were susceptible to oxidation by Fe(III) chloride (E_o = 0.77V) at a molar concentration equivalent to 5 $mg \cdot L^{-1}$ free chlorine (Figure S10). There is a clear change in UV-vis spectra of $Ti_3C_2T_x$ after 10 min of exposure to 5 $mg \cdot L^{-1}$ Fe(III) chloride (Figure S8A). At a higher concentration, 50 $mg \cdot L^{-1}$, the solution becomes colorless in 10 minutes, with evidence of some MXene precipitation under these higher ionic strength conditions

(Figure S8B). In contrast, $Ti_3C_2T_x$ was inert in the less oxidizing environment represented by an oxygen-saturated solution (E_o = 0.40V) (Figure S11).

To determine if the reactivity of MXene towards free chlorine is a consequence of its unique two-dimensional structure, the stability of $Ti_3C_2T_x$ was compared to its closest three-dimensional analog, nanoscale TiC. Experimental details are provided in SI. Similar to $Ti_3C_2T_x$, the spectral envelope in the C 1s region of pristine TiC (Figure S12A) is dominated by a C–Ti peak at 281.5 eV (green band) and a peak at 284.5 eV associated with adventitious carbon. The spectral envelope in the Ti 2p region is a combination of $2p^{3/2}$ and $2p^{1/2}$ peaks at 456 and 461 eV corresponding to Ti-C, and peaks at 458.6 eV and 464.5 associated with TiO_2 (Figure S12B). After 7 days of exposure to 50 $mg \cdot L^{-1}$ free chlorine, conditions sufficient to transform the MXene to crystalline TiO_2 (see Figure 6), no changes in the XPS of nanoscale TiC were observed with the colloidal suspensions remaining black even after a week of exposure to chlorine. This contrasting lack of reactivity towards free chlorine is attributed to the presence of a protective passivating TiO_2 surface layer on the nanoscale TiC; in contrast, MXenes do not possess a protective surface oxide. This difference, combined with the extremely high surface area to volume ratios and the presence of surface defects and under coordinated edges atoms renders MXenes particularly susceptible to oxidative degradation.

ENVIRONMENTAL IMPLICATIONS

To date, the vast majority of MXene studies have focused on developing new environmental technologies (e.g. membranes) and investigating their fate and transport in natural systems.[27,33] In actual use scenarios, more aggressive oxidizing conditions are often encountered; for example, through the addition of chlorine, which is widely used to disinfect water and is part

of the sanitation process for sewage and industrial waste.[42] Normal levels for drinking water disinfection ranges from 0.2 to 4.0 $mg \cdot L^{-1}$ chlorine residuals, and based on the 1st order kinetics we have identified this would correspond to an approximate half-life of 96 to 5 h for MXenes at pH 7, respectively. Chlorination is also commonly used to remove impurities (foulants) that ubiquitously form on membrane surfaces.[43,44] Our results clearly demonstrate that $Ti_3C_2T_x$ MXenes are stable in the presence of sunlight (UVB), UVC rays found in drinking water treatment, and mild oxidizing conditions such as saturated oxygen, but are rapidly oxidized in use scenarios where more aggressive oxidants, namely chlorine, are employed. $Ti_3C_2T_x$ MXenes are degraded to TiO_2 at chlorine concentrations (e.g., 20 $mg \cdot L^{-1}$) much lower than those encountered during membrane backwashing (1000–2000 $mg \cdot L^{-1}$).[69] Thus, for MXenes to be viable in real-world membranes, surface modification processes need to be devised that allow them to remain stable under harsh oxidizing conditions. Previous studies have shown that capping the edges of MXene flakes with polyanions or antioxidants can mitigate the rate of oxidation in aqueous colloidal suspensions by restricting water molecules from otherwise reactive sites.[36,37,70] Another approach could involve surface functionalization, although any successful modification strategy must not compromise desirable MXene properties, most importantly conductivity.

ASSOCIATED CONTENT

Supporting Information

Experimental details, supplementary tables, and figures.

AUTHOR INFORMATION

Corresponding author

D(avid) Howard Fairbrother *Phone: (410) 516-4328; e-mail: howardf@jhu.edu.

ORCID

Nasim Ganji: 0000-0001-6420-908X

Christian A. Reardon-Lochbaum: 0000-0002-1955-2118

Swapnil B. Ambade: 0000-0002-8594-2579

Caroline M. Anastasia: 0000-0001-7478-5574

Patrick Eckhert: 0000-0001-6520-1821

Zeev Rosenzweig: 0000-0001-6098-3932

D. Howard Fairbrother: 0000-0003-4405-9728

Notes

The authors declare no competing financial interest.

ACKNOWLEDGMENTS

This work was supported by the National Science Foundation under Grant No. CHE-2001611, the NSF Center for Sustainable Nanotechnology (CSN). The CSN is part of the Centers for Chemical Innovation Program. The authors gratefully acknowledge the use of facilities and instrumentation supported by the NSF through the University of Wisconsin Water Science and Engineering Laboratory and Materials Research Science and Engineering Center (DMR-1720415). We thank Professor Christopher Shuck and Professor Yuri Gogotsi Group at Drexel University for providing the MAX phase material. We also thank Professor Christina K. Remucal in the Environmental Chemistry and Technology Program at the University of Wisconsin-Madison for assisting in photolysis experiments. This work is dedicated to Dr. Joel Pedersen, who conceived this project but sadly passed away before it came to fruition.

Figures

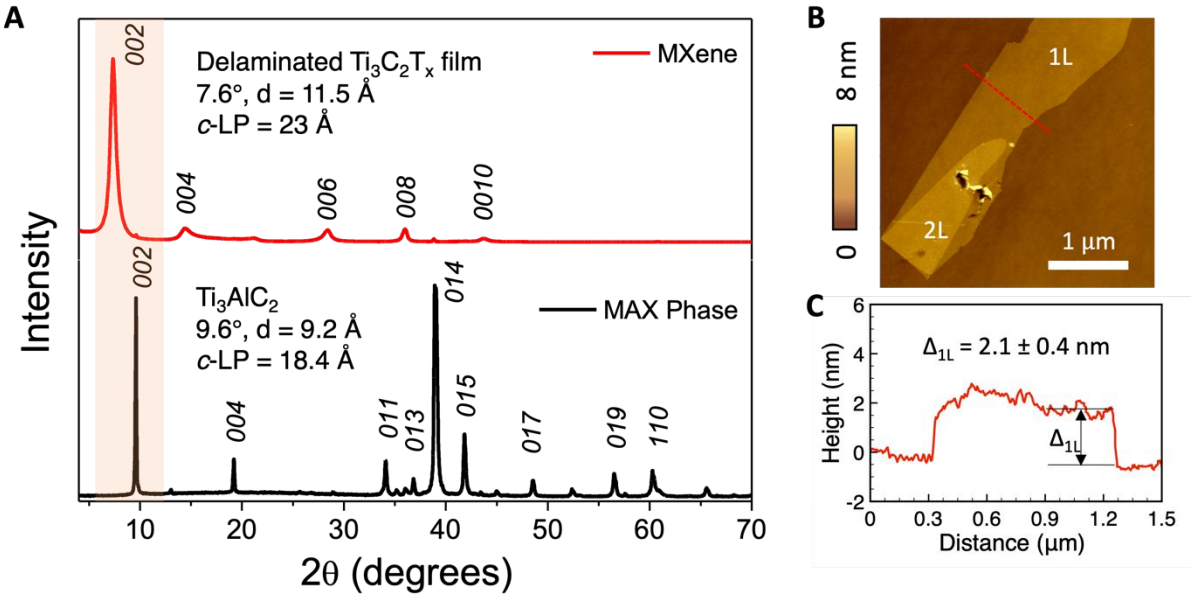

Figure 1. Characterization of $Ti_3C_2T_X$ flakes. (A) XRD spectra of the precursor Ti_3AlC_2 MAX phase (black) and the $Ti_3C_2T_X$ powder (red). (B) AFM images of fresh $Ti_3C_2T_X$ flakes; (C) Height profile along the dashed red line.

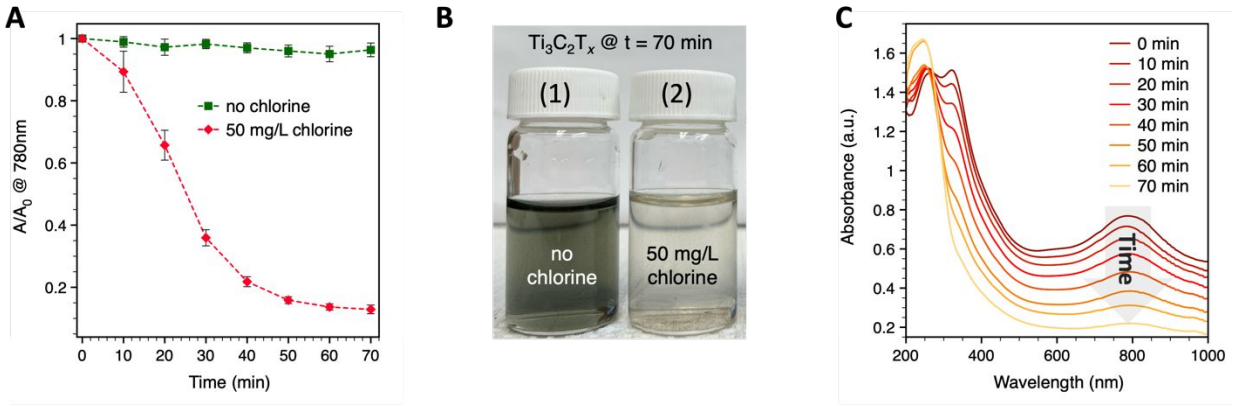

Figure 2. Stability of $Ti_3C_2T_x$ colloidal suspensions (25 mg·L^{-1}) at pH 6 over time. UV-vis spectra of $Ti_3C_2T_x$ suspended (A) with 50 mg·L^{-1} free chlorine over the course of 70 minutes. (B) Representative photographs of $Ti_3C_2T_x$ suspensions with 0 and 50 mg·L^{-1} free chlorine at pH 6 after 70 minutes. (C) Absorbance at 780 nm, normalized to absorbance at the initial time point, for $Ti_3C_2T_x$ solutions with 0 and 50 mg·L^{-1} free chlorine at pH 6 over the course of 70 minutes. All samples were kept open to air at room temperature throughout the experimental timeframe.

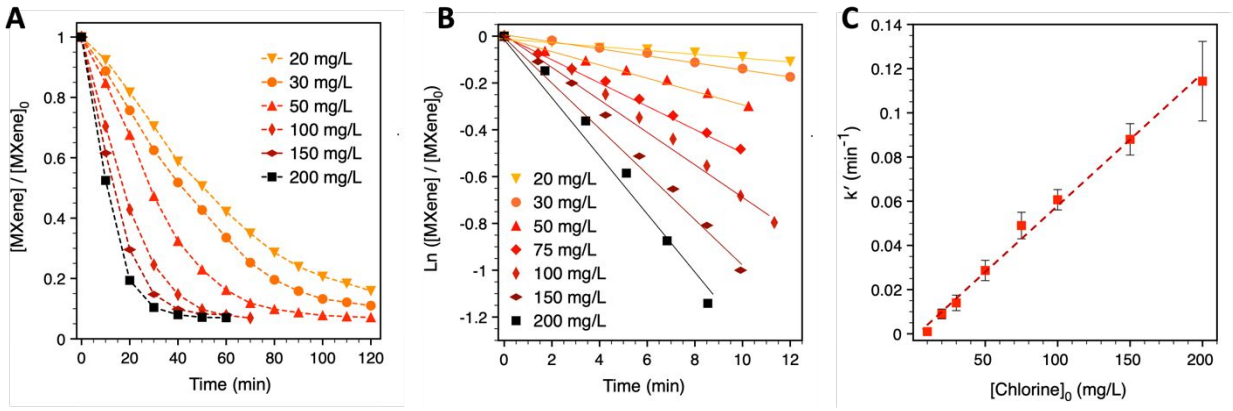

Figure 3. Impact of free chlorine concentration on kinetics of $Ti_3C_2T_x$ degradation. (A) Fraction of $Ti_3C_2T_x$ remaining in solution (obtained from the absorbance at 780 nm) with 20 to 200 mg·L^{-1} free chlorine at pH 6. (B) Initial rates of $Ti_3C_2T_x$ loss in solution (obtained from the absorbance at 780 nm) with 20 to 200 mg·L^{-1} free chlorine at pH 6. The apparent rate constant (k′) for each free chlorine concentration was determined by linear regression of ln([MXene]/[MXene]$_0$) versus time (min). (C) Apparent reaction rate constants (k′) as a function of free chlorine concentration at pH 6. A linear trend line is found between rate constant and chlorine concentration with R^2 of 0.998.

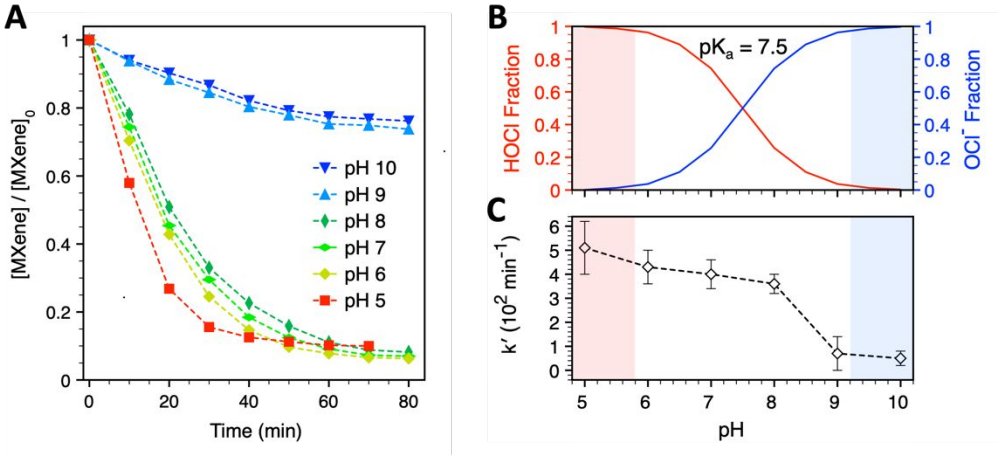

Figure 4. (A) Fraction of $Ti_3C_2T_x$ remaining in solution as a function of time in the presence of 50 $mg \cdot L^{-1}$ free chlorine, plotted for various pH values. (B) Influence of solution pH on the fraction of hypochlorous acid (HOCl) and hypochlorite ion (ClO^-) in water.[49] (C) Reaction rate constants of $Ti_3C_2T_x$ in the presence of 50 $mg \cdot L^{-1}$ free chlorine as a function of solution pH. Error bars represent standard deviation calculated from triplicate experiments. MXene suspensions had starting concentrations of 25 $mg \cdot L^{-1}$. Control studies revealed that in the absence of free chlorine the MXenes remained stable at pH 5 and pH 10 for the 90min time course of these experiments.

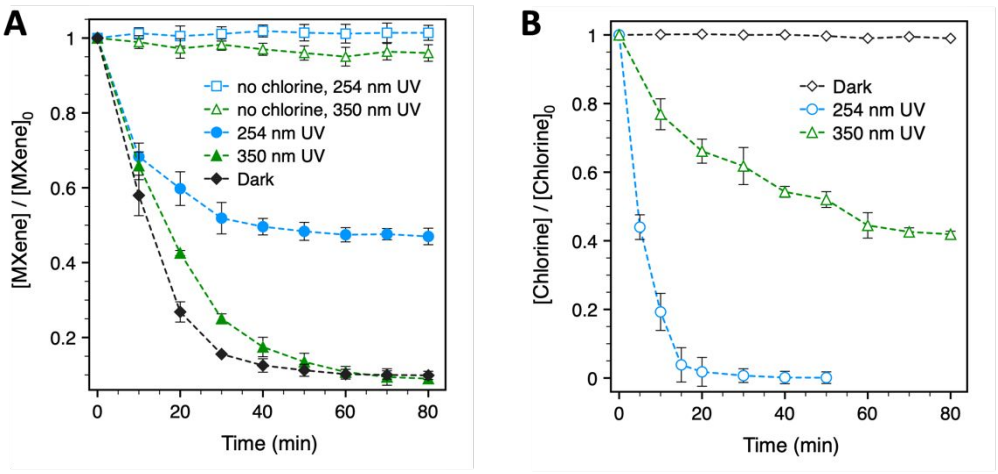

Figure 5. Impact of UV irradiation at 254 nm (7.30 x 10^{-3} mE·cm^{-2}) and 365 nm (6.36 × 10^{-2} mE·cm^{-2}) on chlorine induced phototransformations of $Ti_3C_2T_x$. (A) Fraction of $Ti_3C_2T_x$ remaining in the presence of 0 and 50 mg·L^{-1} free chlorine at pH 6 in dark and under UV irradiation. (B) Fraction of free chlorine remaining in solution (without $Ti_3C_2T_x$) in dark and under UV irradiation. Initial concentration of free chlorine was 50 mg·L^{-1}.

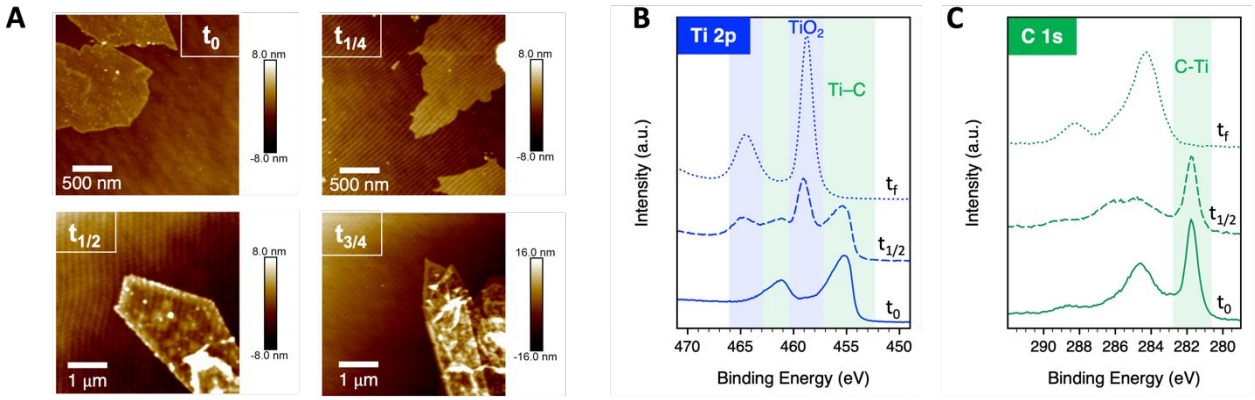

Figure 6. Characterization of $Ti_3C_2T_X$ before and after exposure to 50 mg·L^{-1} free chlorine at pH 6 at varying exposure times using (A) AFM and (B) XPS. Based on UV-Vis data these exposure times corresponded $[MXene]_{(t)}/[MXene]_0 = 1.00, 0.75, 0.50, 0.25$, and ≤ 0.05 values of t_0, $t_{1/4}$, $t_{1/2}$, $t_{3/4}$, and t_f, respectively.

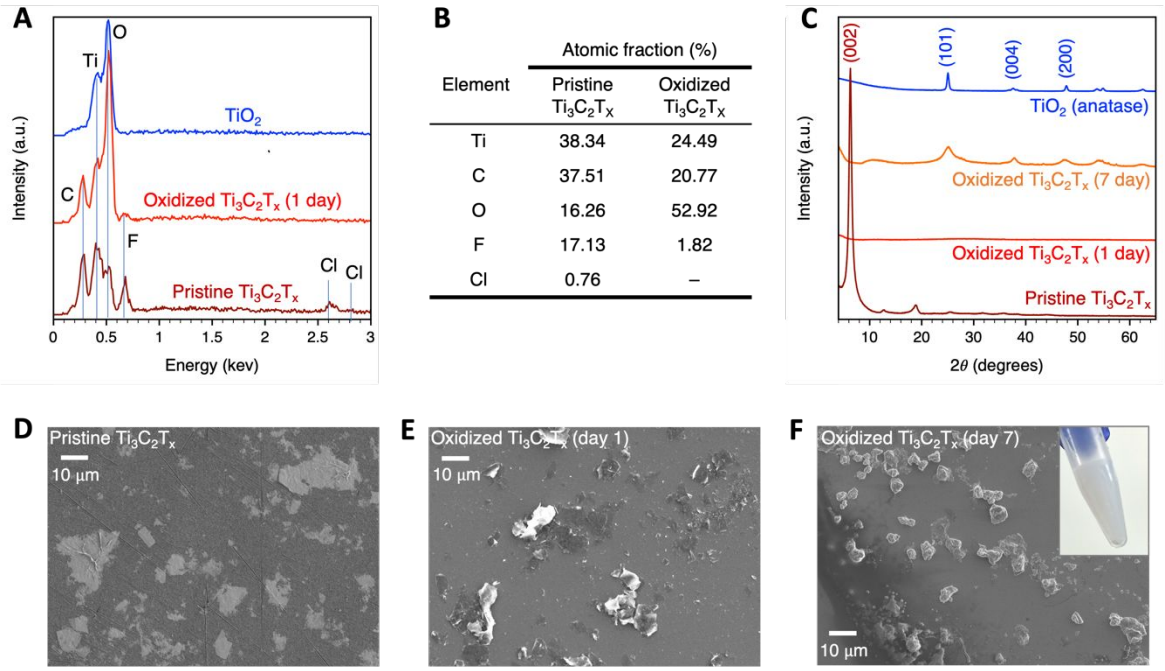

Figure 7. Characterization of $Ti_3C_2T_X$ before (pristine) and after, short (1 day) and long (7 day) exposure to 50 mg·L^{-1} free chlorine at pH 6. (A) Experimental EDS spectra. Full experimental and simulated EDS spectra are presented in Figure S8. (B) Approximate composition of pristine and oxidized $Ti_3C_2T_X$ based on SEM-EDS analysis. (C) XRD patterns of $Ti_3C_2T_X$ before and after 1 day and 7 days of chlorine exposure. SEM images of (D) pristine MXenes and after (E) 1 day and (F) 7 days of chlorination (the insets in (E) shows an image of a concentrated $Ti_3C_2T_x$ suspensions after 7 days of exposure to chlorine).

REFERENCES

(1) Naguib, M.; Mashtalir, O.; Carle, J.; Presser, V.; Lu, J.; Hultman, L.; Gogotsi, Y.; Barsoum, M. W. Two-Dimensional Transition Metal Carbides. *ACS Nano* **2012**, *6* (2), 1322–1331. https://doi.org/10.1021/nn204153h.

(2) Naguib, M.; Kurtoglu, M.; Presser, V.; Lu, J.; Niu, J.; Heon, M.; Hultman, L.; Gogotsi, Y.; Barsoum, M. W. Two-Dimensional Nanocrystals Produced by Exfoliation of Ti3AlC2. *Adv Mater* **2011**, *23* (37), 4248–4253. https://doi.org/10.1002/adma.201102306.

(3) Xie, X.; Chen, C.; Zhang, N.; Tang, Z. R.; Jiang, J.; Xu, Y. J. Microstructure and Surface Control of MXene Films for Water Purification. *Nat Sustain* **2019**, *2* (9), 856–862. https://doi.org/10.1038/s41893-019-0373-4.

(4) Rasool, K.; Pandey, R. P.; Rasheed, P. A.; Buczek, S.; Gogotsi, Y.; Mahmoud, K. A. Water Treatment and Environmental Remediation Applications of Two-Dimensional Metal Carbides (MXenes). *Materials Today*. Elsevier B.V. November 1, 2019, pp 80–102. https://doi.org/10.1016/j.mattod.2019.05.017.

(5) Peng, Q.; Guo, J.; Zhang, Q.; Xiang, J.; Liu, B.; Zhou, A.; Liu, R.; Tian, Y. Unique Lead Adsorption Behavior of Activated Hydroxyl Group in Two-Dimensional Titanium Carbide. *J Am Chem Soc* **2014**, *136* (11), 4113–4116. https://doi.org/10.1021/ja500506k.

(6) Shahzad, A.; Rasool, K.; Miran, W.; Nawaz, M.; Jang, J.; Mahmoud, K. A.; Lee, D. S. Two-Dimensional Ti3C2Tx MXene Nanosheets for Efficient Copper Removal from Water. *ACS Sustain Chem Eng* **2017**, *5* (12), 11481–11488. https://doi.org/10.1021/acssuschemeng.7b02695.

(7) Karthikeyan, P.; Elanchezhiyan, S. S.; Preethi, J.; Talukdar, K.; Meenakshi, S.; Park, C. M. Two-Dimensional (2D) Ti3C2Tx MXene Nanosheets with Superior Adsorption

Behavior for Phosphate and Nitrate Ions from the Aqueous Environment. *Ceram Int* **2021**, *47* (1), 732–739. https://doi.org/10.1016/j.ceramint.2020.08.183.

(8) Jun, B.-M.; Kim, S.; Rho, H.; Park, C. M.; Yoon, Y. Ultrasound-Assisted Ti3C2Tx MXene Adsorption of Dyes: Removal Performance and Mechanism Analyses via Dynamic Light Scattering. *Chemosphere* **2020**, *254*, 126827. https://doi.org/10.1016/j.chemosphere.2020.126827.

(9) Rasool, K.; Helal, M.; Ali, A.; Ren, C. E.; Gogotsi, Y.; Mahmoud, K. A. Antibacterial Activity of Ti3C2Tx MXene. *ACS Nano* **2016**, *10* (3), 3674–3684. https://doi.org/10.1021/acsnano.6b00181.

(10) Meidani, K.; Cao, Z.; Barati Farimani, A. Titanium Carbide MXene for Water Desalination: A Molecular Dynamics Study. *ACS Appl Nano Mater* **2021**, *4* (6), 6145–6151. https://doi.org/10.1021/acsanm.1c00944.

(11) Wang, J.; Chen, P.; Shi, B.; Guo, W.; Jaroniec, M.; Qiao, S.-Z. A Regularly Channeled Lamellar Membrane for Unparalleled Water and Organics Permeation. *Angewandte Chemie* **2018**, *130* (23), 6930–6934. https://doi.org/10.1002/ange.201801094.

(12) Khan, A. R.; Awan, S. K.; Husnain, S. M.; Abbas, N.; Anjum, D. H.; Abbas, N.; Benaissa, M.; Mirza, C. R.; Mujtaba-ul-Hassan, S.; Shahzad, F. 3D Flower like δ-MnO2/MXene Nano-Hybrids for the Removal of Hexavalent Cr from Wastewater. *Ceram Int* **2021**, *47* (18), 25951–25958. https://doi.org/10.1016/j.ceramint.2021.05.326.

(13) Zhang, J.; Kong, N.; Uzun, S.; Levitt, A.; Seyedin, S.; Lynch, P. A.; Qin, S.; Han, M.; Yang, W.; Liu, J.; Wang, X.; Gogotsi, Y.; Razal, J. M. Scalable Manufacturing of Free-Standing, Strong $Ti_3C_2T_x$ MXene Films with Outstanding Conductivity. *Advanced Materials* **2020**, *32* (23), 2001093. https://doi.org/10.1002/adma.202001093.

(14) Gu, S.; Ma, Y.; Zhang, T.; Yang, Y.; Xu, Y.; Li, J. MXene Nanosheet Tailored Bioinspired Modification of a Nanofiltration Membrane for Dye/Salt Separation. *ACS ES&T Water* **2022**. https://doi.org/10.1021/acsestwater.2c00213.

(15) Wu, X.; Ding, M.; Xu, H.; Yang, W.; Zhang, K.; Tian, H.; Wang, H.; Xie, Z. Scalable Ti3C2Tx MXene Interlayered Forward Osmosis Membranes for Enhanced Water Purification and Organic Solvent Recovery. *ACS Nano* **2020**, *14* (7), 9125–9135. https://doi.org/10.1021/acsnano.0c04471.

(16) Bowden, N. B. Nanomaterials-Based Membranes Increase Flux and Selectivity to Enable Chemical Separations. *ACS Appl Nano Mater* **2020**, *3* (10), 9538–9541. https://doi.org/10.1021/acsanm.0c02471.

(17) Lu, Z.; Wei, Y.; Deng, J.; Ding, L.; Li, Z.-K.; Wang, H. Self-Crosslinked MXene (Ti3C2Tx) Membranes with Good Antiswelling Property for Monovalent Metal Ion Exclusion. *ACS Nano* **2019**, *13* (9), 10535–10544. https://doi.org/10.1021/acsnano.9b04612.

(18) Yousaf, T.; Areeb, A.; Murtaza, M.; Munir, A.; Khan, Y.; Waseem, A. Silane-Grafted MXene (Ti3C2Tx) Membranes for Enhanced Water Purification Performance. *ACS Omega* **2022**, *7* (23), 19502–19512. https://doi.org/10.1021/acsomega.2c01143.

(19) Kim, S.; Gholamirad, F.; Shin, B.; Taheri-Qazvini, N.; Cho, J.; Yu, M.; Park, C. M.; Heo, J.; Yoon, Y. Application of a Ti3C2Tx MXene-Coated Membrane for Removal of Selected Natural Organic Matter and Pharmaceuticals. *ACS ES&T Water* **2021**, *1* (9), 2164–2173. https://doi.org/10.1021/acsestwater.1c00242.

(20) Li, Y.; Dai, R.; Zhou, H.; Li, X.; Wang, Z. Aramid Nanofiber Membranes Reinforced by MXene Nanosheets for Recovery of Dyes from Textile Wastewater. *ACS Appl Nano Mater* **2021**, *4* (6), 6328–6336. https://doi.org/10.1021/acsanm.1c01217.

(21) Dong, X.; Bhattacharjee, S.; Zhang, C.; Chai, F. Titanium Carbide-Based Adsorbents for Removal of Heavy Metal Ions and Radionuclides: From Nanomaterials to 3D Architectures. *Adv Mater Interfaces* **2021**, *8* (21), 2100703. https://doi.org/10.1002/admi.202100703.

(22) Ying, Y.; Liu, Y.; Wang, X.; Mao, Y.; Cao, W.; Hu, P.; Peng, X. Two-Dimensional Titanium Carbide for Efficiently Reductive Removal of Highly Toxic Chromium(VI) from Water. *Applied Materials & Interfaces* **2015**, *7*, 1795–1803.

(23) Zhang, Y.; Wang, L.; Zhang, N.; Zhou, Z. Adsorptive Environmental Applications of MXene Nanomaterials: A Review. *RSC Adv* **2018**, *8* (36), 19895–19905. https://doi.org/10.1039/C8RA03077D.

(24) Huang, L.; Ding, L.; Wang, H. MXene-Based Membranes for Separation Applications. *Small Science* **2021**, *1* (7), 2100013. https://doi.org/10.1002/smsc.202100013.

(25) Ren, C. E.; Alhabeb, M.; Byles, B. W.; Zhao, M. Q.; Anasori, B.; Pomerantseva, E.; Mahmoud, K. A.; Gogotsi, Y. Voltage-Gated Ions Sieving through 2d Mxene Ti3c2txmembranes. *ACS Appl Nano Mater* **2018**, *1* (7), 3644–3652. https://doi.org/10.1021/acsanm.8b00762.

(26) Yang, K.; Wang, J.; Chen, X.; Zhao, Q.; Ghaffar, A.; Chen, B. Application of Graphene-Based Materials in Water Purification: From the Nanoscale to Specific Devices. *Environ Sci Nano* **2018**, *5* (6), 1264–1297. https://doi.org/10.1039/C8EN00194D.

(27) Mathis, T. S.; Maleski, K.; Goad, A.; Sarycheva, A.; Anayee, M.; Foucher, A. C.; Hantanasirisakul, K.; Stach, E. A.; Gogotsi, Y. Modified MAX Phase Synthesis for Environmentally Stable and Highly Conductive Ti3C2 MXene. *ACS Nano* **2021**, *15* (4), 6420–6429.

(28) Ren, C. E.; Hatzell, K. B.; Alhabeb, M.; Ling, Z.; Mahmoud, K. A.; Gogotsi, Y. Charge- and Size-Selective Ion Sieving Through Ti3C2Tx MXene Membranes. *Journal of Physical Chemistry Letters* **2015**, *6* (20), 4026–4031. https://doi.org/10.1021/acs.jpclett.5b01895.

(29) Dervin, S.; Dionysiou, D. D.; Pillai, S. C. 2D Nanostructures for Water Purification: Graphene and Beyond. *Nanoscale* **2016**, *8* (33), 15115–15131. https://doi.org/10.1039/C6NR04508A.

(30) Lipatov, A.; Alhabeb, M.; Lukatskaya, M. R.; Boson, A.; Gogotsi, Y.; Sinitskii, A. Effect of Synthesis on Quality, Electronic Properties and Environmental Stability of Individual Monolayer Ti3C2 MXene Flakes. *Adv Electron Mater* **2016**, *2* (12), 1600255. https://doi.org/10.1002/aelm.201600255.

(31) Chae, Y.; Kim, S. J.; Cho, S.-Y.; Choi, J.; Maleski, K.; Lee, B.-J.; Jung, H.-T.; Gogotsi, Y.; Lee, Y.; Ahn, C. W. An Investigation into the Factors Governing the Oxidation of Two-Dimensional Ti3C2 MXene. *Nanoscale* **2019**, *11* (17), 8387–8393. https://doi.org/10.1039/C9NR00084D.

(32) Huang, S.; Mochalin, V. N. Hydrolysis of 2D Transition-Metal Carbides (MXenes) in Colloidal Solutions. *Inorg Chem* **2019**, *58* (3), 1958–1966. https://doi.org/10.1021/acs.inorgchem.8b02890.

(33) Zhang, C. J.; Pinilla, S.; McEvoy, N.; Cullen, C. P.; Anasori, B.; Long, E.; Park, S. H.; Seral-Ascaso, A.; Shmeliov, A.; Krishnan, D.; Morant, C.; Liu, X.; Duesberg, G. S.; Gogotsi, Y.; Nicolosi, V. Oxidation Stability of Colloidal Two-Dimensional Titanium Carbides (MXenes). *Chemistry of Materials* **2017**, *29* (11), 4848–4856. https://doi.org/10.1021/acs.chemmater.7b00745.

(34) Habib, T.; Zhao, X.; Shah, S. A.; Chen, Y.; Sun, W.; An, H.; Lutkenhaus, J. L.; Radovic, M.; Green, M. J. Oxidation Stability of Ti3C2Tx MXene Nanosheets in Solvents and Composite Films. *NPJ 2D Mater Appl* **2019**, *3* (1), 8. https://doi.org/10.1038/s41699-019-0089-3.

(35) Natu, V.; Sokol, M.; Verger, L.; Barsoum, M. W. Effect of Edge Charges on Stability and Aggregation of Ti3C2Tz MXene Colloidal Suspensions. *Journal of Physical Chemistry C* **2018**, *122* (48), 27745–27753. https://doi.org/10.1021/acs.jpcc.8b08860.

(36) Natu, V.; Hart, J. L.; Sokol, M.; Chiang, H.; Taheri, M. L.; Barsoum, M. W. Edge Capping of 2D-MXene Sheets with Polyanionic Salts To Mitigate Oxidation in Aqueous Colloidal Suspensions. *Angewandte Chemie International Edition* **2019**, *58* (36), 12655–12660. https://doi.org/10.1002/anie.201906138.

(37) Zhao, X.; Vashisth, A.; Prehn, E.; Sun, W.; Shah, S. A.; Habib, T.; Chen, Y.; Tan, Z.; Lutkenhaus, J. L.; Radovic, M.; Green, M. J. Antioxidants Unlock Shelf-Stable Ti3C2T (MXene) Nanosheet Dispersions. *Matter* **2019**, *1* (2), 513–526. https://doi.org/10.1016/j.matt.2019.05.020.

(38) Shuck, C. E.; Han, M.; Maleski, K.; Hantanasirisakul, K.; Kim, S. J.; Choi, J.; Reil, W. E. B.; Gogotsi, Y. Effect of Ti3AlC2 MAX Phase on Structure and Properties of Resultant

Ti3C2Tx MXene. *ACS Appl Nano Mater* **2019**, *2* (6), 3368–3376. https://doi.org/10.1021/acsanm.9b00286.

(39) Li, D.; Zou, M.; Jiang, L. Dissolved Oxygen Control Strategies for Water Treatment: A Review. *Water Science and Technology*. IWA Publishing September 15, 2022, pp 1444–1466. https://doi.org/10.2166/wst.2022.281.

(40) Skouteris, G.; Rodriguez-Garcia, G.; Reinecke, S. F.; Hampel, U. The Use of Pure Oxygen for Aeration in Aerobic Wastewater Treatment: A Review of Its Potential and Limitations. *Bioresour Technol* **2020**, *312*. https://doi.org/10.1016/j.biortech.2020.123595.

(41) Sarhan, A. A. O.; Bolm, C. Iron(Iii) Chloride in Oxidative C–C Coupling Reactions. *Chem Soc Rev* **2009**, *38* (9), 2730–2744. https://doi.org/10.1039/b906026j.

(42) Al-Abri, M.; Al-Ghafri, B.; Bora, T.; Dobretsov, S.; Dutta, J.; Castelletto, S.; Rosa, L.; Boretti, A. Chlorination Disadvantages and Alternative Routes for Biofouling Control in Reverse Osmosis Desalination. *npj Clean Water*. Nature Research December 1, 2019. https://doi.org/10.1038/s41545-018-0024-8.

(43) Watts, M. J.; Linden, K. G. Chlorine Photolysis and Subsequent OH Radical Production during UV Treatment of Chlorinated Water. *Water Res* **2007**, *41* (13), 2871–2878. https://doi.org/10.1016/j.watres.2007.03.032.

(44) Neyens, E.; Baeyens, J. *A Review of Classic Fenton's Peroxidation as an Advanced Oxidation Technique*; 2003; Vol. 98.

(45) Chae, H. R.; Lee, J.; Lee, C. H.; Kim, I. C.; Park, P. K. Graphene Oxide-Embedded Thin-Film Composite Reverse Osmosis Membrane with High Flux, Anti-Biofouling, and Chlorine Resistance. *J Memb Sci* **2015**, *483*, 128–135. https://doi.org/10.1016/j.memsci.2015.02.045.

(46) Choi, W.; Choi, J.; Bang, J.; Lee, J. H. Layer-by-Layer Assembly of Graphene Oxide Nanosheets on Polyamide Membranes for Durable Reverse-Osmosis Applications. *ACS Appl Mater Interfaces* **2013**, *5* (23), 12510–12519. https://doi.org/10.1021/am403790s.

(47) Wang, X.; Zhao, Y.; Tian, E.; Li, J.; Ren, Y. Graphene Oxide-Based Polymeric Membranes for Water Treatment. *Advanced Materials Interfaces*. Wiley-VCH Verlag August 9, 2018. https://doi.org/10.1002/admi.201701427.

(48) Watts, M. J.; Linden, K. G. Chlorine Photolysis and Subsequent OH Radical Production during UV Treatment of Chlorinated Water. *Water Res* **2007**, *41* (13), 2871–2878. https://doi.org/10.1016/j.watres.2007.03.032.

(49) Deborde, M.; von Gunten, U. Reactions of Chlorine with Inorganic and Organic Compounds during Water Treatment—Kinetics and Mechanisms: A Critical Review. *Water Res* **2008**, *42* (1–2), 13–51. https://doi.org/10.1016/j.watres.2007.07.025.

(50) Wang, C.; Shang, C.; Ni, M.; Dai, J.; Jiang, F. (Photo)Chlorination-Induced Physicochemical Transformation of Aqueous Fullerene n C60. *Environ Sci Technol* **2012**, *46* (17), 9398–9405. https://doi.org/10.1021/es301037f.

(51) Ambade, S. B.; Kesner, L. A.; Abdel-Rahman, M. K.; Fairbrother, D. H.; Rosenzweig, Z. Interactions of Ti3C2 MXene with Aqueous Zwitterionic Biological Buffers and Their Impact on MXene Properties [Manuscript Submitted for Publication]. *ACS Applied Nano Materials* **2023**.

(52) Bulman, D. M.; Mezyk, S. P.; Remucal, C. K. The Impact of PH and Irradiation Wavelength on the Production of Reactive Oxidants during Chlorine Photolysis. *Environ Sci Technol* **2019**, *53* (8), 4450–4459. https://doi.org/10.1021/acs.est.8b07225.

(53) Wang, D.; Bolton, J. R.; Hofmann, R. Medium Pressure UV Combined with Chlorine Advanced Oxidation for Trichloroethylene Destruction in a Model Water. *Water Res* **2012**, 4677–4686.

(54) Koh, H.-J.; Kim, S. J.; Maleski, K.; Cho, S.-Y.; Kim, Y.-J.; Ahn, C. W.; Gogotsi, Y.; Jung, H.-T. Enhanced Selectivity of MXene Gas Sensors through Metal Ion Intercalation: In Situ X-Ray Diffraction Study. *ACS Sens* **2019**, *4* (5), 1365–1372. https://doi.org/10.1021/acssensors.9b00310.

(55) Li, G.; Tan, L.; zhang, Y.; Wu, B.; Li, L. Highly Efficiently Delaminated Single-Layered MXene Nanosheets with Large Lateral Size. *Langmuir* **2017**, *33* (36), 9000–9006. https://doi.org/10.1021/acs.langmuir.7b01339.

(56) Mashtalir, O.; Naguib, M.; Mochalin, V. N.; Dall'Agnese, Y.; Heon, M.; Barsoum, M. W.; Gogotsi, Y. Intercalation and Delamination of Layered Carbides and Carbonitrides. *Nat Commun* **2013**, *4* (1), 1716. https://doi.org/10.1038/ncomms2664.

(57) Naguib, M.; Unocic, R. R.; Armstrong, B. L.; Nanda, J. Large-Scale Delamination of Multi-Layers Transition Metal Carbides and Carbonitrides "MXenes." *Dalton Transactions* **2015**, *44* (20), 9353–9358. https://doi.org/10.1039/C5DT01247C.

(58) Lipatov, A.; Alhabeb, M.; Lukatskaya, M. R.; Boson, A.; Gogotsi, Y.; Sinitskii, A. Effect of Synthesis on Quality, Electronic Properties and Environmental Stability of Individual Monolayer Ti3C2 MXene Flakes. *Adv Electron Mater* **2016**, *2* (12), 1600255. https://doi.org/10.1002/aelm.201600255.

(59) Maleski, K.; Ren, C. E.; Zhao, M. Q.; Anasori, B.; Gogotsi, Y. Size-Dependent Physical and Electrochemical Properties of Two-Dimensional MXene Flakes. *ACS Appl Mater Interfaces* **2018**, *10* (29), 24491–24498. https://doi.org/10.1021/acsami.8b04662.

(60) Maleski, K. Solution Processing and Optical Properties of 2D Transition Metal Carbides (MXenes), Drexel University, 2019. https://doi.org/10.17918/1q0w-rv44.

(61) An, S.; Wu, J.; Nie, Y.; Li, W.; Fortner, J. D. Free Chlorine Induced Phototransformation of Graphene Oxide in Water: Reaction Kinetics and Product Characterization. *Chemical Engineering Journal* **2020**, *381*, 122609. https://doi.org/10.1016/j.cej.2019.122609.

(62) Morris, J. C. The Acid Ionization Constant of HOCl from 5 to 35°. *J Phys Chem* **1966**, *70* (12), 3798–3805. https://doi.org/10.1021/j100884a007.

(63) Wang, T. X.; Margerum, D. W. Kinetics of Reversible Chlorine Hydrolysis: Temperature Dependence and General-Acid/Base-Assisted Mechanisms. *Inorg Chem* **1994**, *33* (6), 1050–1055. https://doi.org/10.1021/ic00084a014.

(64) Wu, J.; Benoit, D.; Lee, S. S.; Li, W.; Fortner, J. D. Ground State Reactions of NC60 with Free Chlorine in Water. *Environ Sci Technol* **2016**, *50* (2), 721–731. https://doi.org/10.1021/acs.est.5b04368.

(65) Hou, W. C.; Chowdhury, I.; Goodwin, D. G.; Henderson, W. M.; Fairbrother, D. H.; Bouchard, D.; Zepp, R. G. Photochemical Transformation of Graphene Oxide in Sunlight. *Environ Sci Technol* **2015**, *49* (6), 3435–3443. https://doi.org/10.1021/es5047155.

(66) Zhao, Y.; Liu, Y.; Zhang, X.; Liao, W. Environmental Transformation of Graphene Oxide in the Aquatic Environment. *Chemosphere*. Elsevier Ltd January 1, 2021. https://doi.org/10.1016/j.chemosphere.2020.127885.

(67) Cao, X.; Zhao, J.; Wang, Z.; Xing, B. New Insight into the Photo-Transformation Mechanisms of Graphene Oxide under UV-A, UV-B and UV-C Lights. *J Hazard Mater* **2021**, *403*. https://doi.org/10.1016/j.jhazmat.2020.123683.

(68) Hu, K.; Xie, X.; Szkopek, T.; Cerruti, M. Understanding Hydrothermally Reduced Graphene Oxide Hydrogels: From Reaction Products to Hydrogel Properties. *Chemistry of Materials* **2016**, *28* (6), 1756–1768. https://doi.org/10.1021/acs.chemmater.5b04713.

(69) Tin, M. M. M.; Anioke, G.; Nakagoe, O.; Tanabe, S.; Kodamatani, H.; Nghiem, L. D.; Fujioka, T. Membrane Fouling, Chemical Cleaning and Separation Performance Assessment of a Chlorine-Resistant Nanofiltration Membrane for Water Recycling Applications. *Sep Purif Technol* **2017**, *189*, 170–175. https://doi.org/10.1016/j.seppur.2017.07.080.

(70) Huang, S.; Natu, V.; Tao, J.; Xia, Y.; Mochalin, V. N.; Barsoum, M. W. Understanding the Effect of Sodium Polyphosphate on Improving the Chemical Stability of Ti3C2Tz MXene in Water. *J Mater Chem A Mater* **2022**, *10* (41), 22016–22024. https://doi.org/10.1039/d2ta04009c.